01 Nov 2014

Fully Differential Study of Interference Effects in the Ionization of H_2 by Proton Impact

Sachin D. Sharma

T. P. Arthanayaka

Ahmad Hasan
Missouri University of Science and Technology, hasana@mst.edu

B. R. Lamichhane

et. al. For a complete list of authors, see https://scholarsmine.mst.edu/phys_facwork/1312

Recommended Citation

S. D. Sharma et al., "Fully Differential Study of Interference Effects in the Ionization of H_2 by Proton Impact," *Physical Review A - Atomic, Molecular, and Optical Physics*, vol. 90, no. 5, pp. 052710-1-052710-8, American Physical Society (APS), Nov 2014.
The definitive version is available at https://doi.org/10.1103/PhysRevA.90.052710

Fully differential study of interference effects in the ionization of H_2 by proton impact

S. Sharma,[1] T. P. Arthanayaka,[1] A. Hasan,[1,2] B. R. Lamichhane,[1] J. Remolina,[1] A. Smith,[1] and M. Schulz[1]
[1]*Department of Physics and LAMOR, Missouri University of Science and Technology, Rolla, Missouri 65409, USA*
[2]*Department of Physics, UAE University, P.O. Box 15551, Al Ain, Abu Dhabi, United Arab Emirates*
(Received 3 May 2014; revised manuscript received 29 September 2014; published 12 November 2014)

We have measured fully differential cross sections for ionization of H_2 by 75-keV proton impact. The coherence length of the projectile beam was varied by changing the distance between a collimating slit and the target. By comparing the cross sections measured for large and small coherence lengths pronounced interference effects could be identified in the data. A surprising result is that the phase angle in the interference term is primarily determined by the momentum transfer and only to a lesser extent by the recoil-ion momentum.

DOI: 10.1103/PhysRevA.90.052710 PACS number(s): 34.50.Fa, 34.50.Bw

I. INTRODUCTION

Over the last 10–15 years kinematically complete experiments (i.e., experiments which determine the momentum vectors of all particles in the system under investigation) revealed that the description of the spatial and temporal evolution of systems as simple as two positively charged ions interacting with an electron represent a formidable theoretical challenge [e.g., 1–12]. The basic problem is that the Schrödinger equation is not analytically solvable for more than two mutually interacting particles, even when the underlying forces are precisely known. This dilemma is known as the few-body problem (FBP). As a result, theory has to resort to approximations and numeric approaches. Even for a simple system containing only three particles the theoretical codes can become very complex, and realistically modeling an exact solution is only possible with the aid of very large computational efforts and resources. For ionization of atoms and molecules by ion impact, calculations are particularly challenging because of the large projectile mass, which means that an enormous number of angular momentum states of the incoming and outgoing projectiles has to be accounted for. Indeed, qualitative discrepancies between calculated and measured fully differential cross sections (FDCS) for ionization of helium were observed even in the case of very fast projectiles [e.g., 1,6,12], which were thought to represent a relatively "easy" case. For smaller projectile speeds, and especially for larger charge states, the discrepancies become even larger [e.g., 3,4,9].

After a decade of vivid debates a possible explanation, based on the projectile coherence properties, for some of these surprising discrepancies was offered [13]. Earlier, interference structures in the ejected electron spectra [e.g., 14,15], in the scattering angle dependence of double differential cross sections [16], and in the molecular orientation dependent cross section for ionization of or capture from molecular hydrogen [17] were reported. This interference was interpreted as being due to indistinguishable electron ejection [14,15] or diffraction of the projectile wave [16] from the two atomic centers in the molecule. However, later it was argued that interference effects in the scattering angle dependence are only present if the projectile beam is coherent, i.e., if the coherence length is larger than the dimension of the diffracting object [13]. It was further argued that in ionization of atomic targets different types of interference (e.g., between first- and higher-order transition amplitudes) can be present, but that here, too, the coherence requirements must be satisfied. While fully quantum-mechanical models assumed a fully coherent beam, the transverse coherence length realized in the experiment reported in Ref. [1] (and in many other fully differential measurements) was much smaller than the size of the target atom. Later, this explanation for the discrepancies between experiment and theory was supported by FDCS measured for a projectile beam with a much larger transverse coherence length [18], for which the discrepancies were significantly reduced.

The findings on the role of projectile coherence reported in Ref. [13] have led to further intense discussions. Feagin and Hargreaves argued that the difference in the data between the coherent and incoherent beams presented in Ref. [13] should not be seen as a wave-packet coherence effect [19]. Instead, they asserted that the effects observed in Ref. [13] are due to an incoherent superposition of an ensemble of projectiles originating from an extended source. In a recent experimental study we tested their theoretical analysis and found that it was not (or at least not fully) supported by our data [20]. There, we analyzed the angular resolution of the detected projectiles and experimentally determined that the resolutions for the supposedly coherent and incoherent beams did not differ significantly. In contrast, Feagin and Hargreaves had to assume that the resolution for the incoherent beam had to be substantially worse (nearly by an order of magnitude) in order to reproduce the experimental data. The results of [20] thus demonstrate that the differences in the cross sections for different slit distances are not merely due to an experimental resolution effect.

In Ref. [20] we also found indications that the phase angle entering in the interference term is not primarily determined by the recoil-ion momentum, which was believed to be the case for two-center molecular interference, but rather by the transverse component of the momentum transfer **q** from the projectile to the target. These observations, as well as the theoretical analysis of [19], show that further investigations of the role of the projectile coherence and interference effects in ionization of molecular hydrogen are needed. In this article we report a fully differential study of interference effects in target ionization by ion impact. The data support our previous interpretation that the projectile coherence properties generally can have a significant impact on the collision cross

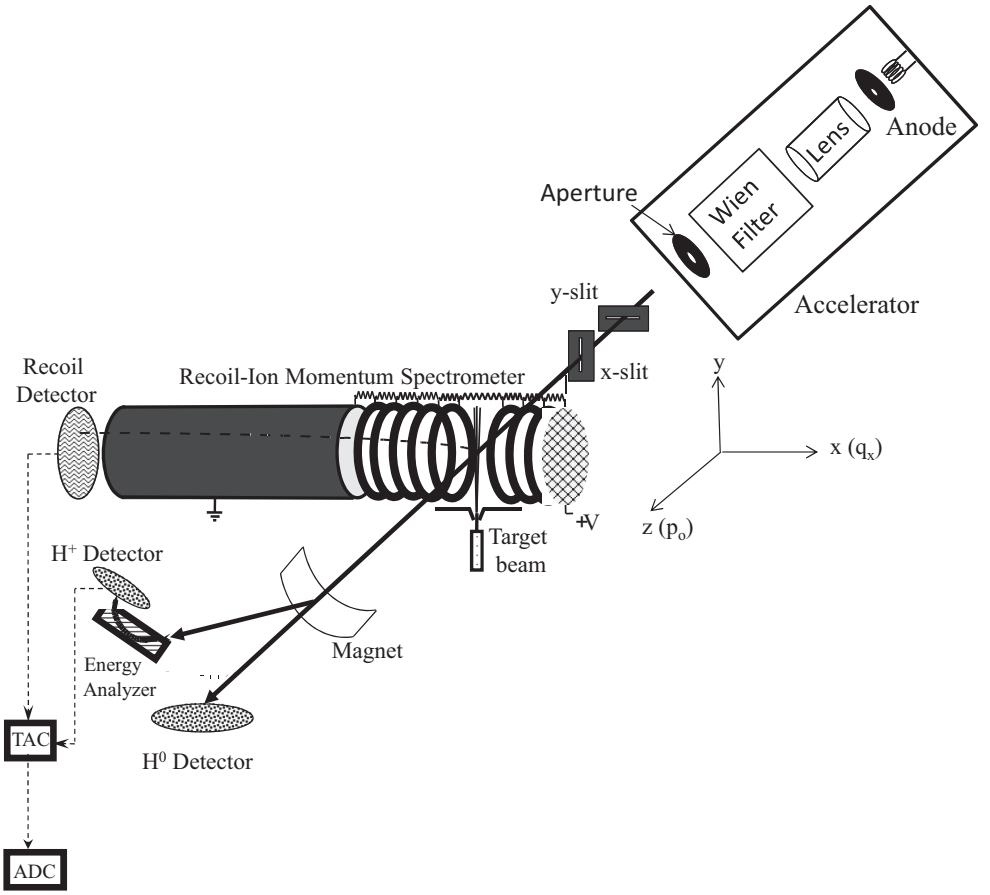

FIG. 1. Schematic diagram of the experimental setup. The recoil ions, momentum analyzed by the recoil-ion momentum spectrometer, were measured in coincidence with the scattered projectiles, which were momentum analyzed by the parallel-plate energy analyzer. The vertical collimation slit (x slit) was placed at a variable distance to the target in order to vary the transverse coherence length.

sections. Furthermore, the present data confirm that the phase angle in the interference term is primarily determined by the transverse momentum transfer.

II. EXPERIMENTAL SETUP

The experiment was performed at the projectile- and recoil-ion momentum spectrometer facility at Missouri S&T. A sketch of the setup is shown in Fig. 1, where it should be noted that the dimensions of the various components are not shown to scale. A proton beam was generated with a hot cathode ion source (where the cathode is a filament) and extracted through an anode aperture with a diameter of 0.5 mm to an energy of 5 keV. The beam was focused by an electrostatic lens and cleaned from components other than 5-keV protons by a Wien filter. It was then collimated by a second aperture 1.5 mm in diameter and located about 45 cm from the lens at the end of the accelerator terminal. After acceleration to an energy of 75 keV the proton beam was further collimated in the x direction with a vertical slit of width 150 μm located at a variable distance of approximately 100–150 cm from the aperture. A second slit, oriented horizontally, used to collimate the beam in the y direction (also with a width of 150 μm), was kept at a fixed distance from the target (a few millimeters from the large-distance location of the x slit). The collimated proton beam was then intersected with a very cold ($T \cong 1$–2 K) neutral H_2 beam generated by a supersonic gas jet.

The transverse coherence length Δr of the projectiles at the target is given by [21]

$$\Delta r = (L/2a)\,\lambda, \tag{1}$$

where a is the width of the slit, L its distance to the target, and λ is the de Broglie wavelength. The coherence length was varied by placing the collimating slit at two different distances ($L_1 = 6.5$ cm, $L_2 = 50$ cm) from the target. Without the slit Δr at the target is determined by the geometry of the aperture at the end of the accelerator terminal. The distance between the aperture and the end of the acceleration region is short (about 25 cm) so that the change in λ, relative to λ corresponding to 75 keV, does not have a significant effect on Δr. Overall, without the slit Δr is about 1 a.u. With the slit placed at L_1 Eq. (1) would yield $\Delta r = 0.43$ a.u. However, since the slit can only increase, but not decrease Δr, at the small distance Δr is the same as without the slit. With the slit placed at L_2, Eq. (1) yields $\Delta r = 3.3$ a.u. In this context it should be emphasized that an "undamped" interference structure is only observable for $\Delta r = \infty$. The ratio between the intensities in the interference maxima and minima (referred to as the "visibility" by Michelson [22]) systematically decreases with decreasing Δr. Therefore, the cross sections measured for different Δr

can differ even if the smaller Δr is larger than the size of the diffracting object.

It should further be noted that the size of the interaction volume is very small. In the two directions perpendicular to the proton beam it is given by the width of the projectile beam, which at the target is less than 0.2 mm. Strictly speaking, the coherence length depends on the location of the target molecule, from which the projectile is diffracted, within this dimension. However, for this very small size the effect on Δr is negligible. Likewise, the length of the target along the projectile beam axis ($\cong$1 mm) is less than 2% of the slit distance to the target (even for the small distance) and its effect on the coherence length is therefore negligible as well. Furthermore, it should be noted that the finite size of the interaction volume would reduce Δr and the effect would be larger for the small slit distance than for the large slit distance so that the change in coherence length between both distances would even be larger.

The projectiles which did not charge exchange in the collision were selected by a switching magnet, decelerated by 70 keV, and energy analyzed by an electrostatic parallel-plate analyzer [23]. The beam component which suffered an energy loss of 30 eV was detected by a two-dimensional position-sensitive channel-plate detector. From the position information in the x direction (defined by the orientation of the analyzer entrance and exit slits) the x component of $\mathbf{q}$ could be determined. Because of the very narrow width of the analyzer slits (75 μm) the y component of $\mathbf{q}$ was fixed at 0 for all detected projectiles. The z component (pointing in the projectile beam direction) of $\mathbf{q}$ is given by $q_z = \varepsilon/v_p$, where ε and v_p are the energy loss and the speed of the projectiles. The resolution in the x, y, and z components of $\mathbf{q}$ was 0.32, 0.2, and 0.07 a.u. full width at half maximum (FWHM), respectively.

The H_2^+ ions produced in the collisions were extracted by a weak electric field of 8 V/cm and then drifted in a field-free region, twice as long as the extraction region, before hitting another two-dimensional position-sensitive channel-plate detector. From the position information the y and z components of the recoil-ion momentum could be determined. The two detectors were set in coincidence and the coincidence time is, apart from a constant offset, equal to the time of flight of the recoil ions from the collision region to the detector. From it, the x component of the recoil-ion momentum can

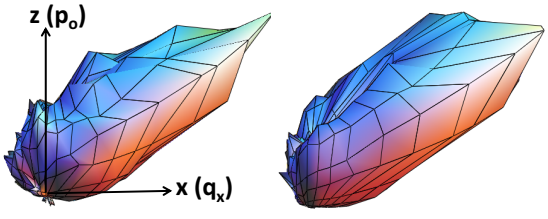

FIG. 2. (Color online) Fully differential, three-dimensional angular distribution of ejected electrons with an energy of 14.6 eV taken for the large (left panel) and small (right panel) slit distance and for a momentum transfer of 0.9 a.u. p_o indicates the initial projectile momentum, which defines the positive z axis. q_x is the transverse component of the momentum transfer, which defines the positive x axis.

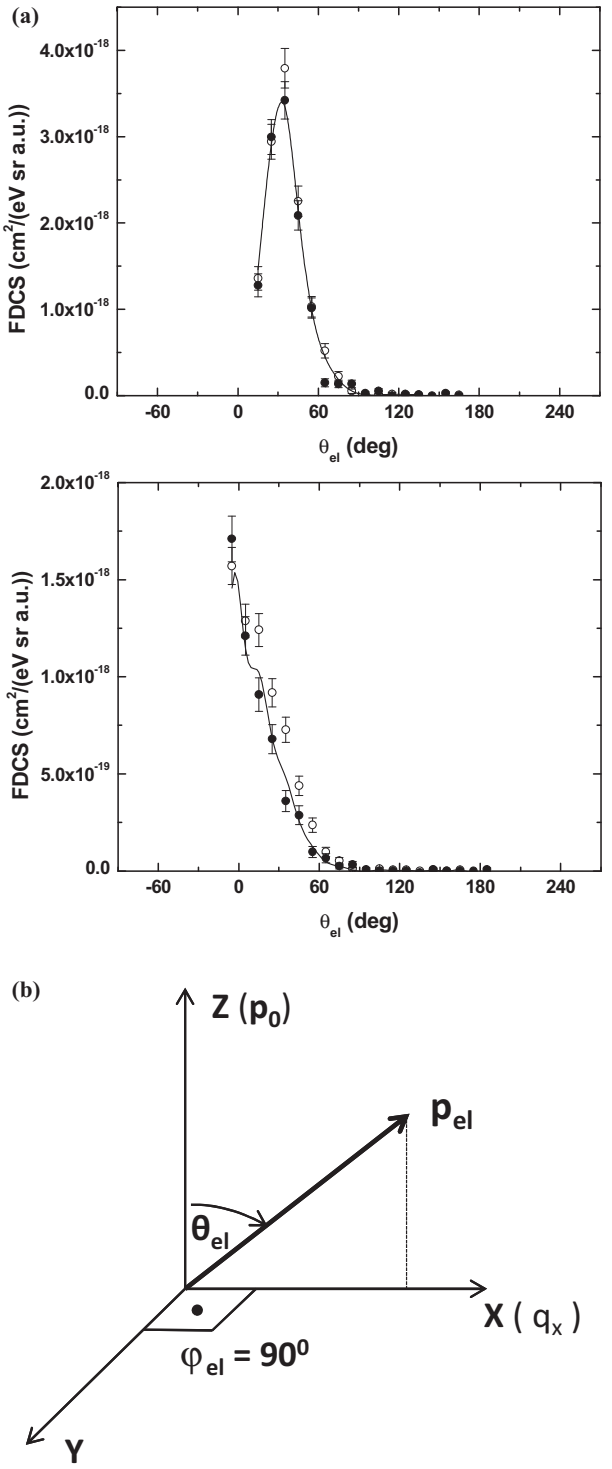

FIG. 3. (a) Fully differential cross sections for electrons ejected into the scattering plane as a function of the polar emission angle. The x component of the recoil-ion momentum was fixed at -0.2 a.u. (top panel) and $+0.2$ a.u. (bottom panel). The closed (open) symbols represent the data taken for the large (small) slit distance. The solid lines represent the product of the incoherent data with an interference term of the form $1 + \alpha\cos(q_x D)$ (see text for details). (b) Illustration of the electron ejection geometry for the FDCS plotted in panel (a). Only electrons ejected into the scattering plane (xz plane), defined by p_o and q_x, are analyzed, i.e., the azimuthal angle φ_{el} is fixed at 90° and the polar angle θ_{el}, measured relative to the z axis, is varied.

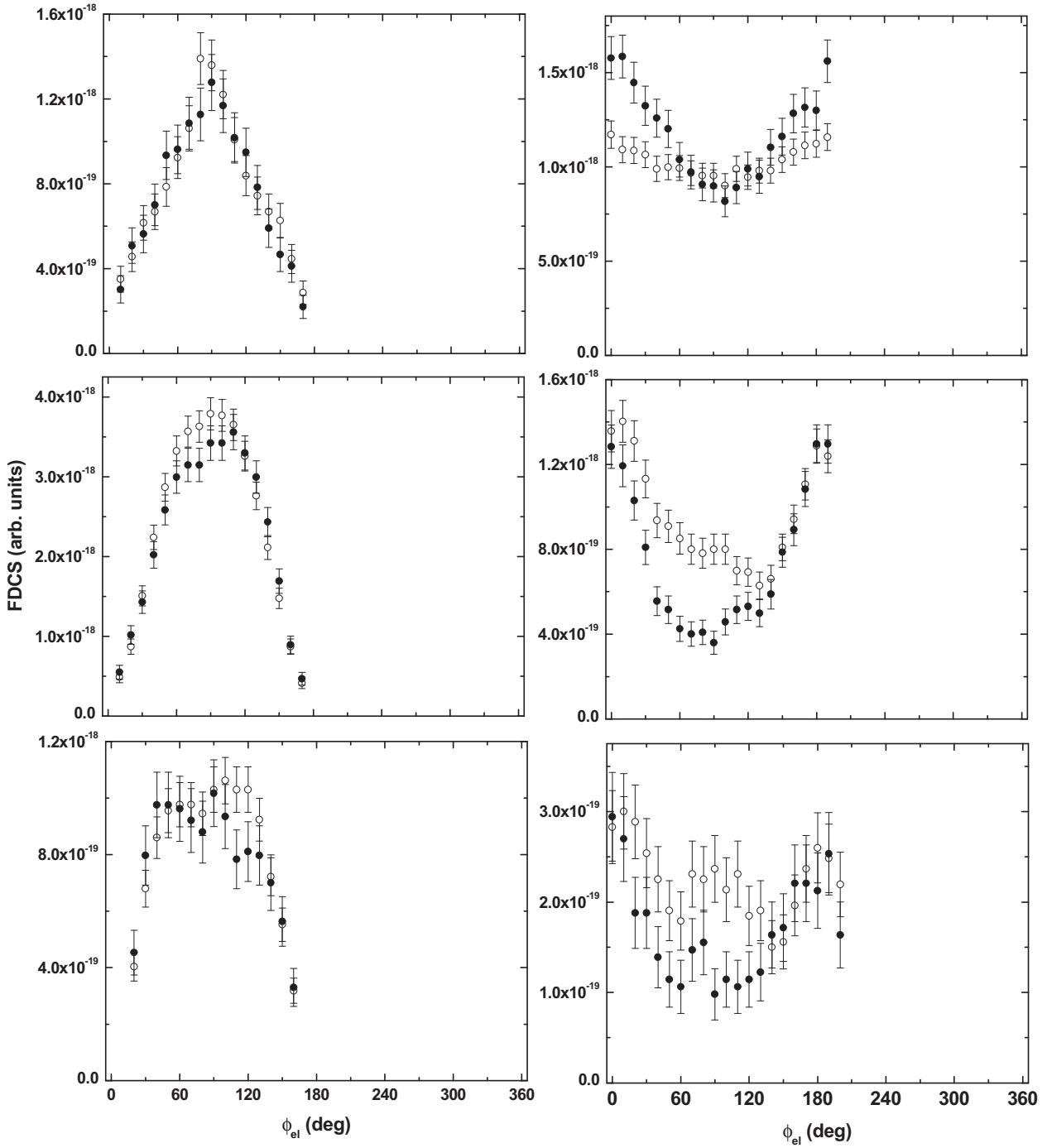

FIG. 4. Fully differential cross sections as a function of the azimuthal electron ejection angle for fixed polar angles of 15° (top panels), 35° (center panels), and 55° (bottom panels). The x component of the recoil-ion momentum was fixed at -0.2 a.u. (left panels) and $+0.2$ a.u. (right panels). Symbols as in Fig. 3. For a sketch of the ejection geometry see Fig. 5.

be determined. The momentum resolution in the x, y, and z directions was 0.15, 0.5, and 0.15 a.u. FWHM, respectively. Finally, the electron momentum was deduced from momentum conservation by $\mathbf{p_{el}} = \mathbf{q} - \mathbf{p_{rec}}$.

III. RESULTS AND DISCUSSION

The FDCS can be presented in many different ways. One common method, originally introduced to present FDCS for ionization by electron impact (for a review see, e.g., [24]) and later adopted for ion impact (for a review see, e.g., [25]) is to fix the magnitude of $\mathbf{q}$ (or equivalently the projectile scattering angle) and the ejected electron energy and to plot the FDCS as a function of the azimuthal and polar electron emission angles φ_{el} and θ_{el}. Here, θ_{el} is measured relative to the projectile beam axis and φ_{el} relative to the positive y axis; i.e., $\varphi_{el} - 90^\circ$ is the angle relative to the transverse component of $\mathbf{q}$ (which in our coordinate system is equal to its x component q_x). An

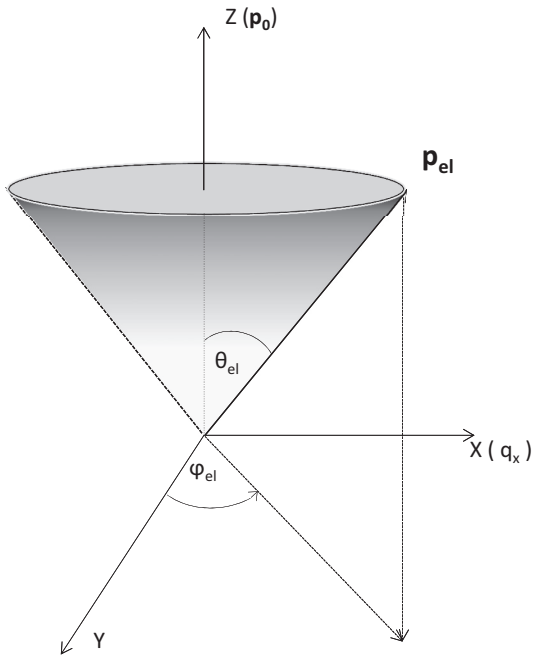

FIG. 5. Illustration of the electron ejection geometry for the FDCS plotted in Fig. 4. The polar angle θ_{el} is fixed at 15° (top panels), 35° (center panels), and 55° (bottom panels). Therefore, for all electrons analyzed in Fig. 4 the momentum vectors lie on the surface of a cone with an opening angle of $2\theta_{el}$ centered on the z axis. The FDCS are plotted as a function of the azimuthal angle φ_{el}, which is the angle between the projection of the electron momentum onto the xy plane and the positive y axis.

example of such three-dimensional fully differential angular distributions of the ejected electrons is shown in Fig. 2 for $q = 0.9$ a.u. The data in the left panel were taken for the large slit distance and those in the right panel for the small slit distance. As far as the shape of the angular dependence is concerned, only relatively small differences between these two data sets were observed. These differences occur mostly outside the scattering plane, spanned by the initial and final projectile momenta, where the FDCS maximize.

The similarity between the spectra of Fig. 2 for small and large slit distances is consistent with the conclusion reported in Ref. [20] that the phase angle in the interference term is not primarily determined by the recoil momentum, but rather by q_x. Since q_x is fixed in the data of Fig. 2 the angular shape of the FDCS should then not be affected much by the interference term. Therefore, in order to extract detailed information about the phase angle from the data it is advantageous to find a representation of the FDCS in which q_x changes with φ_{el} and/or θ_{el}. One possibility is to generate the fully differential electron angular distribution for a fixed x component of $\mathbf{p_{rec}}$ rather than for fixed q (which is equivalent to fixing q_x because $q_y = 0$ and q_z is constant for a fixed electron energy). In such a presentation each set of φ_{el} and θ_{el} corresponds to a different q_x according to

$$q_x = p_{recx} + p_{el} \sin\varphi_{el} \sin\theta_{el}. \quad (2)$$

In Fig. 3 the FDCS for p_{recx} fixed at -0.2 a.u. (top panel) and $+0.2$ a.u. (bottom panel) are shown for electrons ejected into the scattering plane as a function of θ_{el} (i.e., φ_{el} is fixed at 90°). Here, we are using a nonconventional coordinate system in which θ_{el} varies between 0° and 360° and φ_{el} between 0° and 180°. For the angular range 0°–180° the x component of the electron momentum is parallel to q_x. It should be noted that the positive x direction is determined by q_x; i.e., by choice of the coordinate system $q_x < 0$ is not possible. Therefore, only the angular ranges 11°–169° and −11°–191° are possible for $p_{recx} = -0.2$ a.u. and $p_{recx} = 0.2$ a.u., respectively; outside these regions $q_x < 0$. The data represented by the closed symbols were taken for the large slit distance and those represented by the open symbols for the small slit distance. In the case of $p_{recx} = -0.2$ a.u. no significant differences in the angular dependence of both data sets are found. However, for $p_{recx} = 0.2$ a.u. and in the angular range $\theta_{el} \cong 15°$–75° the FDCS for the coherent beam are systematically smaller than for the incoherent beam.

One disadvantage of analyzing interference effects in the FDCS for electrons ejected into the scattering plane is that here the angular electron distribution is sharply peaked, especially for $p_{recx} = -0.2$ a.u. As a result, the variation of the phase angle in the interference term is limited to a narrow range for which data can be collected with sufficient statistics. In order to avoid this problem we also analyzed the azimuthal angular dependence of the FDCS for fixed polar angles of the ejected electrons. Here, we switch back to conventional spherical coordinates in which θ_{el} runs from 0° to 180° and φ_{el} from 0° to 360°. Since the FDCS are very small for $\theta_{el} > 60°$ we present the φ_{el} dependence of the FDCS for (from top to bottom) $\theta_{el} = 15°$, 35°, and 55° and for $p_{recx} = -0.2$ a.u. (left panels) and $p_{recx} = 0.2$ a.u. (right panels) in Fig. 4. The electron ejection geometry is illustrated in Fig. 5. Fixing θ_{el} means that only electrons are selected for which the momentum vector lies on the surface of a cone with an opening angle $2\theta_{el}$ centered on the z axis. In Fig. 4 too, as in Fig. 3, the angular ranges for which no data are shown are kinematically not allowed because $q_x < 0$. In this representation of the data the structures in the FDCS are much broader than in the θ_{el} dependence for electrons ejected into the scattering plane. Once again, for $p_{recx} = -0.2$ a.u. only small, but for $p_{recx} = 0.2$ a.u. significant differences between the FDCS for the coherent and incoherent beams can be seen.

The ratio R between the cross sections for the large and small slit distances represents the interference term, as outlined in Ref. [13], even if the beam is still coherent for the small distance (see comment regarding the visibility in the experimental section). In the following we analyze to what extent the measured ratios are consistent with the FDCS being affected by interference effects. R is plotted as a function of φ_{el} in Fig. 6 for the same kinematic settings (and in the same order) as for the FDCS of Fig. 4. The horizontal error bars show the angular resolution of the ejected electrons, which was estimated using a Monte Carlo simulation [26].

Two trends are seen in Fig. 6: First, the interference structure is more pronounced for positive than for negative p_{recx}, at least for $\theta_{el} = 15°$ and 35°. Second, the interference structure tends to be more pronounced at large θ_{el}. Since for fixed values of θ_{el}, p_{recx}, and of the electron energy, φ_{el} unambiguously determines q_x, the variation of the interference term with φ_{el} implies that the phase angle depends on q_x. In Ref. [20] we showed that within a simple, geometric

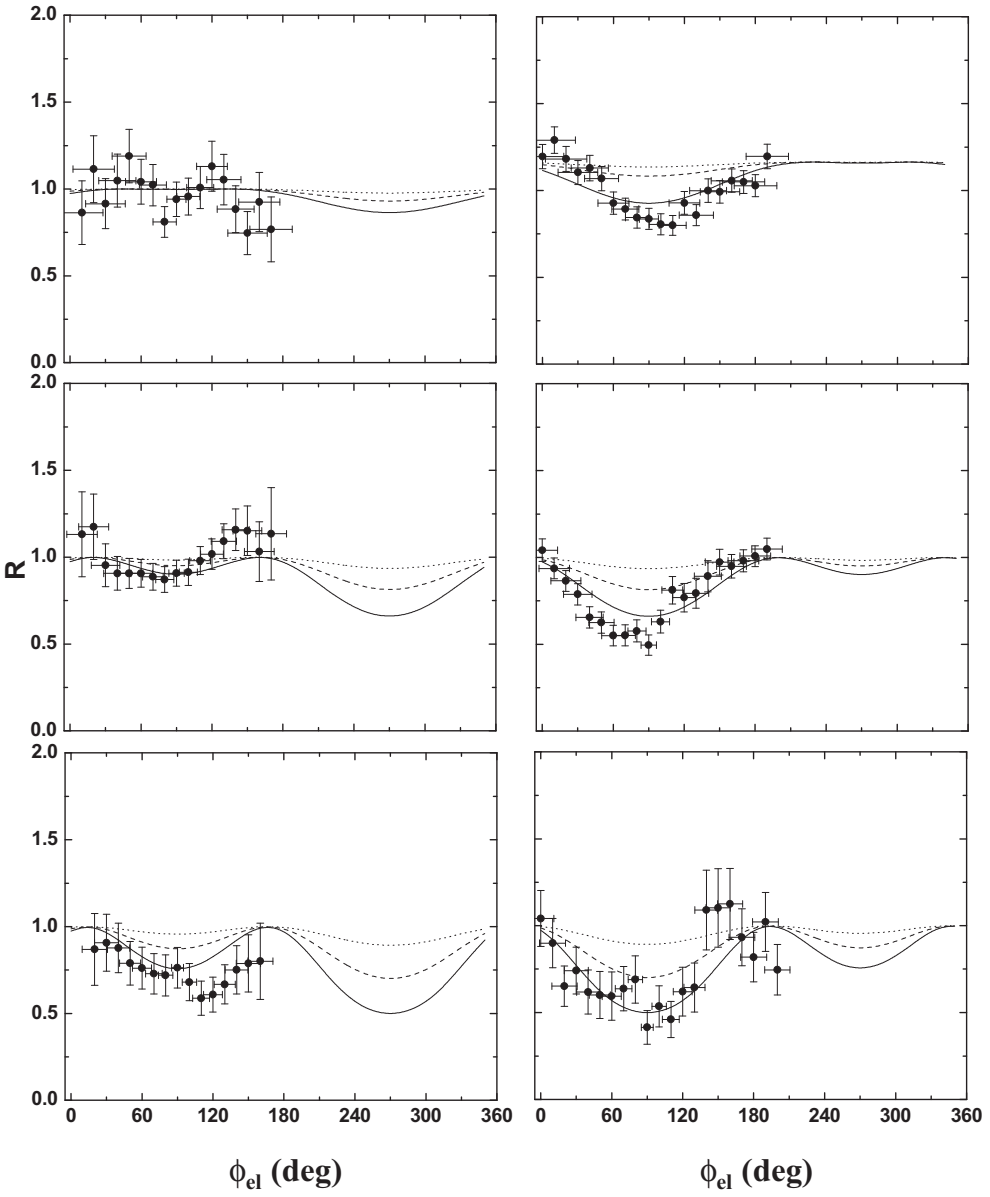

FIG. 6. Fully differential cross-section ratios between the large and small slit distance data of Fig. 4. The solid and dashed lines were obtained from $1+\alpha\cos(q_x D)$ and Eq. (1) with $D = 2$ and 1.4 a.u., respectively, and the dotted curve from $1+\alpha\sin(q_x D)/(q_x D)$ and $D = 1.4$ a.u. In each case $\alpha = 0.5$.

model the position of the interference extrema in the measured scattering angle dependence of the double differential cross-section ratios between the coherent and incoherent beams can be fitted quite well by an interference term of the form $I = 1+\alpha\cos(q_x D)$ with $D = 2$ a.u. and $\alpha = 0.5$. This relation, with q_x determined from Eq. (2), is shown in Fig. 6 as the solid curves. The constant α in I accounts for the "damping" of the interference due to incomplete coherence even for the large slit distance and due to experimental resolution effects. In all cases the measured R are very well reproduced by this calculated I. The same interference term, multiplied by the incoherent FDCS, also reproduces the coherent FDCS for the scattering plane plotted in Fig. 3 (solid curves). This supports the conclusion of Ref. [20] suggesting that the phase angle in the interference term is primarily determined by q_x.

One important question to be answered is what implication of the dominance of q_x in the phase angle may be drawn regarding the type of interference that leads to the structures in R. As mentioned above, originally we believed that the interference was due to indistinguishable diffraction of the projectile wave from the two atomic centers in the molecule [13,16]. In this case the interference term was thought to be given by [27]

$$I = 1 + \cos(\mathbf{p_{rec}} \cdot \mathbf{d}) \tag{3a}$$

or

$$I = 1 + \sin(p_{\rm rec} d)/(p_{\rm rec} d), \tag{3b}$$

depending on whether the molecular orientation is fixed or random. Here, **d** is the internuclear separation vector. Neither expression reproduces our measured R.

In Ref. [20] we considered two possibilities to explain this observation. First, the phase angle in molecular two-center interference may not be primarily determined by $\mathbf{p_{rec}}$, but rather by q_x. But even then the dimension of the diffracting structure should still be given by the internuclear distance d, which is 1.4 a.u. for H_2. Second, the dominant contribution to the interference may be due to some type other than two-center molecular interference. More specifically, we considered the possibility of first- and higher-order ionization amplitudes interfering with each other (to which we referred as single-center interference). Such interference contributions were reported in coherent calculations [8,11]. The impact parameters that contribute to the cross section at a specific scattering angle tend to be larger for first-order than for higher-order processes. This type of interference can therefore also be interpreted as due to different (and indistinguishable) impact parameters leading to the same scattering angle. The requirement for observable interference is then that the transverse coherence length must be larger than the separation in the impact-parameter distribution for the first- and higher-order contributions.

In order to test whether the FDCS are sensitive enough to distinguish between single- and two-center interference, in Fig. 6 expressions (3a) and (3b), with $\mathbf{p_{rec}}$ replaced by q_x and $d = 1.4$ a.u. and the damping factor α inserted, are plotted as dashed and dotted curves, respectively. Equation (3a) assumes that the molecule is always aligned along q_x, which yields the most pronounced interference structure. Since the molecular orientation is not measured and we do not know whether the orientation is random, the measured R should be compared to the region between the dashed and dotted curves.

In most cases, the data seem to favor $D = 2$ a.u., i.e., single-center interference. However, the differences between both dimensions are not of sufficient significance to base a firm conclusion on them. Furthermore, it should be kept in mind that the data of Ref. [20] suggested a rather weak, but not an absent dependence of the phase angle on p_{rec}. Therefore, a third possibility is that both two-center molecular (with the phase angle being determined by $\mathbf{p_{rec}}$) and single-center interferences are present in the data. The data strongly suggest that in this case the contributions from the latter would be larger.

IV. CONCLUSIONS AND OUTLOOK

In summary, we have performed a fully differential study of interference effects in ionization of H_2. Differences in the measured cross sections depending on the transverse coherence length are confirmed by the present data. The ratio between the fully differential angular distributions of the ejected electrons for fixed energy and recoil-ion momentum for a coherent and an incoherent beam can be well described by an interference term in which the phase angle is primarily determined by the transverse projectile momentum transfer. However, the FDCS are not sensitive enough to distinguish between two-center molecular and single-center interference. In order to shed more light on this important point we will perform further fully differential measurements varying kinematic parameters: First, we plan to repeat the experiment for a larger projectile energy loss and for a different initial projectile energy. Both parameters should have an effect on the impact-parameter range contributing to ionization and thereby on the phase angle for single-center interference, while the internuclear separation of the molecule, which enters in the phase angle for two-center interference, is not affected. Second, we will measure FDCS for ionization of helium using proton beams of varying coherence length, for which molecular two-center interference obviously cannot contribute.

ACKNOWLEDGMENT

This work was supported by the National Science Foundation under Grant No. PHY-1401586.

[1] M. Schulz, R. Moshammer, D. Fischer, H. Kollmus, D. H. Madison, S. Jones, and J. Ullrich, Nature **422**, 48 (2003).
[2] R. Dörner, H. Khemliche, M. H. Prior, C. L. Cocke, J. A. Gary, R. E. Olson, V. Mergel, J. Ullrich, and H. Schmidt-Böcking, Phys. Rev. Lett. **77**, 4520 (1996).
[3] N. V. Maydanyuk, A. Hasan, M. Foster, B. Tooke, E. Nanni, D. H. Madison, and M. Schulz, Phys. Rev. Lett. **94**, 243201 (2005).
[4] M. Schulz, R. Moshammer, A. N. Perumal, and J. Ullrich, J. Phys. B **35**, L161 (2002).
[5] A. L. Harris, D. H. Madison, J. L. Peacher, M. Foster, K. Bartschat, and H. P. Saha, Phys. Rev. A **75**, 032718 (2007).
[6] M. McGovern, C. T. Whelan, and H. R. J. Walters, Phys. Rev. A **82**, 032702 (2010).
[7] J. Colgan, M. S. Pindzola, F. Robicheaux, and M. F. Ciappina, J. Phys. B **44**, 175205 (2011).
[8] A. B. Voitkiv, B. Najjari, and J. Ullrich, J. Phys. B **36**, 2591 (2003).
[9] R. T. Pedlow, S. F. C. O'Rourke, and D. S. F. Crothers, Phys. Rev. A **72**, 062719 (2005).
[10] M. F. Ciappina and W. R. Cravero, J. Phys. B **39**, 1091 (2006).
[11] X. Y. Ma, X. Li, S. Y. Sun, and X. F. Jia, Europhys. Lett. **98**, 53001 (2012).
[12] K. A. Kouzakov, S. A. Zaytsev, Yu. V. Popov, and M. Takahashi, Phys. Rev. A **86**, 032710 (2012).
[13] K. N. Egodapitiya, S. Sharma, A. Hasan, A. C. Laforge, D. H. Madison, R. Moshammer, and M. Schulz, Phys. Rev. Lett. **106**, 153202 (2011).
[14] N. Stolterfoht, B. Sulik, V. Hoffmann, B. Skogvall, J. Y. Chesnel, J. Rangama, F. Fremont, D. Hennecart, A. Cassimi, X. Husson, A. L. Landers, J. A. Tanis, M. E. Galassi, and R. D. Rivarola, Phys. Rev. Lett. **87**, 023201 (2001).
[15] D. Misra, U. Kadhane, Y. P. Singh, L. C. Tribedi, P. D. Fainstein, and P. Richard, Phys. Rev. Lett. **92**, 153201 (2004).

[16] J. S. Alexander, A. C. Laforge, A. Hasan, Z. S. Machavariani, M. F. Ciappina, R. D. Rivarola, D. H. Madison, and M. Schulz, Phys. Rev. A **78**, 060701(R) (2008).
[17] D. Misra, H. T. Schmidt, M. Gudmundsson, D. Fischer, N. Haag, H. A. B. Johansson, A. Källberg, B. Najjari, P. Reinhed, R. Schuch, M. Schöffler, A. Simonsson, A. B. Voitkiv, and H. Cederquist, Phys. Rev. Lett. **102**, 153201 (2009).
[18] X. Wang, K. Schneider, A. LaForge, A. Kelkar, M. Grieser, R. Moshammer, J. Ullrich, M. Schulz, and D. Fischer, J. Phys. B **45**, 211001 (2012).
[19] J. M. Feagin and L. Hargreaves, Phys. Rev. A **88**, 032705 (2013).
[20] S. Sharma, T. P. Arthanayaka, A. Hasan, B. R. Lamichhane, J. Remolina, A. Smith, and M. Schulz, Phys. Rev. A **89**, 052703 (2014).
[21] C. Keller, J. Schmiedmayer, and A. Zeilinger, Opt. Commun. **179**, 129 (2000).
[22] A. A. Michelson. Philos. Mag. **30**, 1 (1890).
[23] A. D. Gaus, W. Htwe, J. A. Brand, T. J. Gay, and M. Schulz, Rev. Sci. Instrum. **65**, 3739 (1994).
[24] H. Ehrhardt, K. Jung, G. Knoth, and P. Schlemmer, Z. Phys. D **1**, 3 (1986).
[25] M. Schulz and D. H. Madison, Int. J. Mod. Phys. A **21**, 3649 (2006).
[26] M. Dürr, B. Najjari, M. Schulz, A. Dorn, R. Moshammer, A. B. Voitkiv, and J. Ullrich, Phys. Rev. A **75**, 062708 (2007).
[27] S. E. Corchs, R. D. Rivarola, J. H. McGuire, and Y. D. Wang, Phys. Scr. **50**, 469 (1994).